Revista Mexicana de Astronomía y Astrofísica, **48**, 149–157 (2012)

THE UNIVERSAL TIME-EVOLUTION OF AN EXPANDING HII REGION

A. C. Raga,[1] J. Cantó,[2] and L. F. Rodríguez[3]

Received 2011 November 11; accepted 2012 February 15

RESUMEN

Presentamos nuevos modelos de la expansión de una región HII dentro de un medio uniforme. Con un modelo de capa delgada y con simulaciones hidrodinámicas (+transporte radiativo) con simetría esférica, demostramos que las regiones HII observadas están en un intervalo de parámetros para el cual existe una solución adimensional universal. Esta ley universal se deriva de los modelos de capa delgada y de las simulaciones numéricas. Una comparación entre estos dos tipos de modelos muestra que el formalismo de capa delgada sólo es válido para las fases tempranas de la expansión de una región HII. Finalmente, tabulamos la "ley universal" (derivada de las simulaciones hidrodinámicas) y damos una aproximación analítica a esta ley, la cual puede ser escalada para obtener el radio en función del tiempo de cualquier región HII observada.

ABSTRACT

We present new models for the expansion of an HII region into a uniform environment. With a thin-shell model and with full, gasdynamic (+radiative transfer), spherically symmetric simulations, we demonstrate that observed HII regions are in a parameter regime for which there is a universal, dimensionless expansion law. This universal expansion solution is derived from the thin shell model and from the numerical simulations. A comparison between the two types of model shows that the thin shell formalism is valid only for the early phases of the HII region expansion. Finally, we tabulate the "universal law" (derived from the spherically symmetric simulations) and give an analytic approximation to this law, which can be scaled to obtain the radius vs. time of any observed HII region.

Key Words: HII regions — ISM: evolution — ISM: kinematics and dynamics — stars: formation

1. INTRODUCTION

The timescale for "normal" (i.e., low density) HII regions to reach pressure equilibrium with the surrounding environment is longer than the lifetime of the O stars which power them. However, the more recently discovered "compact", "ultracompact", and even "hypercompact" HII regions (the more extreme of which have sizes $\leq$0.03 pc and are embedded in molecular clouds with densities $>10^6$ cm^{-3}, see Kurtz 2005) do reach pressure equilibrium (and stop expanding) while their central star is still on the main sequence (de Pree, Rodríguez, & Goss 1995).

These observational developments have brought new life to theoretical studies of expanding HII regions. Quite extensive work has been done in the past on numerical (e.g., Mathews & O'Dell 1969; Tenorio-Tagle et al. 1982) and analytic (Franco, Tenorio-Tagle, & Bodenheimer 1990; Shu et al. 2002) solutions to the expanding HII region problem. The observations of compact HII regions (see above) led Raga, Cantó, & Rodríguez (2012) to focus on the regime of relaxation of the HII region expansion to its final, pressure equilibrium. In the present paper, we pursue this line of work.

The general characteristics of the problem are as follows. As described, e.g., in the book of Dyson & Williams (1980), after an instantaneous "turning on" of a stellar source (with an S_* ionizing photon rate) in a homogeneous environment, an HII region first undergoes a constant density expansion until it

[1]Instituto de Ciencias Nucleares, Universidad Nacional Autónoma de México, D.F., Mexico.

[2]Instituto de Astronomía, Universidad Nacional Autónoma de México, D.F., Mexico.

[3]Centro de Radioastronomía y Astrofísica, Universidad Nacional Autónoma de México, Morelia, Michoacán, Mexico.

reaches its "initial Strömgren radius",

$$R_S = \left(\frac{3S_*}{4\pi n_0^2 \alpha_{\rm H}} \right)^{1/3}, \qquad (1)$$

where n_0 is the hydrogen number density of the neutral environment and $\alpha_{\rm H}$ is the case B recombination coefficient of H.

When this radius is approached, the HII region begins a slower "hydrodynamic expansion", in which the hot, ionized gas expands, incorporates more material, and pushes out the surrounding, neutral environment. This expansion continues until the HII region reaches a final radius

$$R_f = \frac{R_S}{\sigma^{2/3}}, \qquad (2)$$

where $\sigma = (c_0/c_i)^2$, with c_0 and c_i being the isothermal sound speeds of the neutral and the ionized gas, respectively. It could be argued that instead of the sound speeds, it might be appropriate to use (in the definition of σ) a "turbulent velocity" characteristic of small scale turbulent motions. However, such turbulent velocities would be of the order of the local sound speed, so that the value of σ is not likely to be modified very strongly.

When the HII region reaches R_f, the pressure of the inner, ionized region is equal to the pressure of the outer, neutral environment. As the photoionized region has a temperature $\sim 10^4$ K and the outer, neutral environment a temperature $\sim$10–100 K, we have $\sigma \sim 0.001 - 0.01$, so that $R_f \sim 20 - 100\ R_S$.

Spitzer (1968) and later Dyson & Williams (1980) constructed an analytic model (which we will call "Dyson's solution", in memory of Dyson's enlightened discussion of this problem) for the expansion of an HII region, based on the assumption of pressure balance between the ionized region and the neutral, shocked gas (pushed out by the HII region). This model has recently been improved by Raga et al. (2012), so that it correctly relaxes to the final, pressure equilibrium radius R_f (see equation 2).

Raga et al. (2012) show that their analytic model fails to produce the "overexpansion" obtained in gasdynamic, HII region simulations, and claim that this failure is due to the fact that the analytic model does not incorporate the inertia of the shocked, neutral gas. In the present paper we discuss a "thin shell model" which does include the inertia of the neutral gas pushed out by the expanding region (§ 2). We also present 1D spherical, gasdynamic simulations, with which we evaluate the validity of the thin shell model (§ 3). The results of this comparison are summarized in § 4.

2. THE THIN SHELL MODEL

2.1. *The general problem*

Let us consider a model for the expansion of an HII region with the following regions:

- an inner, photoionized region which we assume to be uniform (in density and temperature), with an isothermal sound speed c_i ($\approx$10 km s^{-1}),
- a thin, spherical shell of neutral material which is pushed out by the expanding HII region,
- a surrounding, undisturbed, neutral environment with a uniform density n_0 and isothermal sound speed c_0 ($\approx$1 km s^{-1}).

We then write an equation for the time-evolution of the mass M of the thin shell:

$$\frac{dM}{dt} = \left(4\pi R^2 n_0 v - \dot{N}_{\rm ion} \right) m, \qquad (3)$$

and an equation for its momentum Mv:

$$\frac{d}{dt}\left(Mv\right) = 4\pi R^2 \left(P_i - P_0\right), \qquad (4)$$

where R is the radius and $v = dR/dt$ the velocity of the thin shell, m is the mass per atom/ion ($= m_{\rm H}$ for a pure H gas), P_i is the pressure of the HII region and P_0 is the pressure of the undisturbed, neutral environment. The mass M and ionization rate $\dot{N}_{\rm ion}$ of the thin shell obey the relations

$$M = \frac{4\pi}{3} R^3 (n_0 - n) m, \qquad (5)$$

and

$$\dot{N}_{\rm ion} = S_* - \frac{4\pi}{3} R^3 n^2 \alpha_{\rm H}, \qquad (6)$$

where n is the (uniform) ion number density of the HII region and $\alpha_{\rm H} \approx 2.59 \times 10^{-13}$ cm^3 s^{-1} is the case B recombination coefficient of H at 10^4K.

We now define the dimensionless variables:

$$r = \frac{R}{R_S}, \quad n' = \frac{n}{n_0}, \quad \text{and} \quad t' = \frac{t c_i}{R_S}. \qquad (7)$$

Equations (3–6) can then be combined to obtain a system of two differential equations involving these dimensionless variables:

$$\frac{d}{dt'}\left(r^3 n'\right) = \lambda \left(1 - r^3 n'^2\right), \qquad (8)$$

$$\frac{d}{dt'}\left[r^3 (1 - n') \frac{dr}{dt'} \right] = 3\left(n' - \sigma\right) r^2, \qquad (9)$$

where

$$\sigma \equiv \left(\frac{c_0}{c_i}\right)^2; \qquad \lambda \equiv \frac{R_s n_0 \alpha_{\rm H}}{c_i}, \tag{10}$$

with R_S given by equation (1). The λ parameter is the ratio of the sound crossing time (R_S/c_i) over the recombination time of the initial Strömgren sphere ($1/n_o\alpha_{\rm H}$). Therefore, for large values of λ, the evolutionary timescale of the HII region (initially $\approx R_S/c_i$ since the expansion begins at an approximately sonic velocity) is much longer than the recombination timescale (which can be used as an estimate for the time in which the nebula reaches photoionization equilibrium).

Since $c_i \approx 10$ km s^{-1} and $c_0 \approx 1$ km s^{-1} (see above), we have $\sigma \approx 0.01$. Combining equations (10) and (1) we obtain

$$\lambda = \frac{1}{c_i}\left(\frac{3S_* n_0 \alpha_{\rm H}^2}{4\pi}\right)^{1/3} = 54.30 \times \left(\frac{S_*}{10^{49}{\rm s}^{-1}}\right)^{1/3}\left(\frac{n_0}{1\,{\rm cm}^{-3}}\right)^{1/3}\left(\frac{10\,{\rm km\,s}^{-1}}{c_i}\right). \tag{11}$$

Therefore, for HII regions driven by sources with ionizing photon rates $S_* \sim 10^{49}$ s^{-1} into uniform environments with densities $n_0 \geq 1$ cm^{-3}, we will always have $\lambda > 50$.

The initial radius of the shell (formed at the end of the initial, constant density expansion of the ionization front) is $R = R_S$ (i.e., $r = 1$) and the initial value of the HII region density is $n = n_0$ (i.e., $n' = 1$). Expanding equations (8–9) around these initial values, it is straightforward to show that the initial expansion velocity v_i of the shell is

$$v_i = c_i\sqrt{1-\sigma} \qquad \rightarrow \qquad \frac{dr}{dt'} = \sqrt{1-\sigma}\,. \tag{12}$$

With these initial values, equations (8–9) can be integrated in a straightforward way to obtain $R(t)$ and $n(t)$.

In Figure 1, we show the shell radius as a function of time obtained for $\sigma = 0.01$ (see equation 10) and for $\lambda = 10$, 10^2, 10^3 and 10^4, spanning the possible values for this dimensionless parameter (see equation 11). The shell radius shows an oscillatory behaviour at long evolutionary times. We will show in § 3 that these oscillations are unphysical.

2.2. *The case of global photoionization equilibrium*

As shown by equation (11), the dimensionless parameter λ has values $\gg$1 for all observed HII regions. This empirical fact implies that the term in parentheses in the right hand side of equation (8) has to have values $\sim\lambda^{-1} \ll 1$. Therefore, we have:

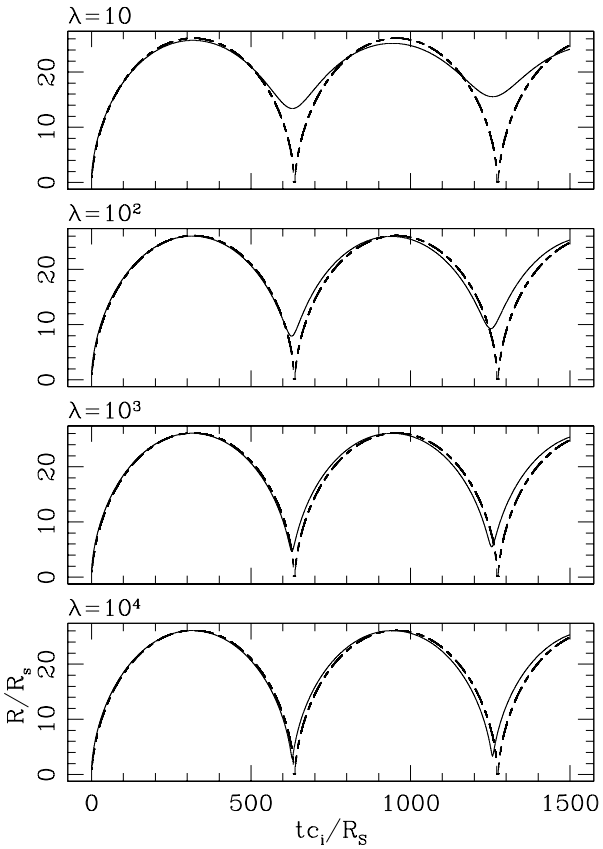

Fig. 1. The solid curves give the HII region radius (in units of R_S) as a function of time (in units of R_S/c_i) obtained from numerical integrations of the thin shell model (equations 8–9) for $\sigma = 0.01$ and for different λ values (each plot is labeled with the corresponding λ value). In all plots, the "high λ solution" (obtained by integrating equation 14 with $\sigma = 0.01$) is shown with a dashed curve. The thin shell solution show a series of oscillations which are unphysical (as discussed in § 3.2).

$$r^3 n'^2 \approx 1 \quad \rightarrow \quad S_* = \frac{4\pi}{3} R^3 n^2 \alpha_{\rm H}\,, \tag{13}$$

the second equality involving the dimensional variables. This is the condition of global balance between the stellar ionizing photon production rate and the recombination rate in the whole volume of the HII region.

We can then substitute equation (13) in equation (9) to obtain:

$$\frac{d^2 r^4}{dt'^2} = 12\left(r^{1/2} - \sigma r^2\right), \tag{14}$$

where we have furthermore assumed that $n \ll n_0$ (which is correct except for the very early evolution of the hydrodynamic expansion of the HII region).

The numerical solution to equation (14) obtained for $\sigma = 0.01$ is plotted in all of the frames of Figure 1, showing that it reproduces well the solutions to the more general problem described by equations (8–9) for all of the considered values of the dimensionless parameter λ. We therefore conclude that for the values of λ corresponding to all observed HII regions (see equation 11), the assumption of global ionization equilibrium (equation 14) leads to a thin shell solution in good agreement with the non-equilibrium formulation (equations 8–9).

For the $\sigma = 0$ case (i.e., $c_0 = 0$, the case of a "cold" surrounding environment), equation (14) has the analytic solution:

$$R(t) = R_S\,(1+at)^{4/7}\,, \quad \text{with} \quad a = \frac{7}{2\sqrt{3}}\frac{c_i}{R_S}\,. \tag{15}$$

Interestingly, this relation is most similar to Dyson's solution (in which the inertia of the expanding, neutral material is neglected, see § 1), which only differs from equation (15) in the constant a, which has a value $a_D = 7c_0/(4R_S)$.

2.3. *The universal $\sigma \ll 1$, $\lambda \gg 1$ solution*

Equation (14) can be rewritten in the form:

$$\frac{d^2}{d\tau^2}\left(\frac{R}{R_f}\right)^4 = 12\left[\left(\frac{R}{R_f}\right)^{1/2} - \left(\frac{R}{R_f}\right)^2\right], \tag{16}$$

where a new dimensionless time $\tau = tc_0/R_f$ has been defined, and $R_f = R_S/\sigma^{2/3}$ is the final, pressure equilibrium radius of the expanding HII region, see equation (2).

This equation has to be integrated with the initial condition $R(t=0) = R_S$, which using equation (2) can be written in the form:

$$\left(\frac{R}{R_f}\right)_{t=0} = \sigma^{2/3}\,,$$
$$\left(\frac{dR/R_f}{d\tau}\right)_{t=0} = \sqrt{\sigma^{-1}-1}\,. \tag{17}$$

This initial condition then introduces the dependence of the solution on the dimensionless parameter σ (see equation 10).

As we have described in § 1, expanding HII regions generally have values $\sigma \gg 1$. Therefore, the initial condition given by equation (17) can be replaced with

$$\left(\frac{R}{R_f}\right)_{t=0} \approx 0\,,$$
$$\left(\frac{dR/R_f}{d\tau}\right)_{t=0} \to \infty\,. \tag{18}$$

Using this modified initial condition, it is possible to integrate equation (17) to obtain a "universal solution", which is correct for all HII region expansion problems with $\sigma \ll 1$ and $\lambda \gg 1$ (see equations 10 and 11). A numerical integration of this problem gives results which are basically indistinguishable from the $\sigma = 0.01$ photoionization equilibrium solution shown in Figure 1.

3. NUMERICAL SIMULATIONS

3.1. *The models*

In order to evaluate the thin shell solutions described above, we have carried out 1D, spherically symmetric simulations of an expanding HII region, integrating the set of equations:

$$\frac{\partial n}{\partial t} + \frac{\partial nu}{\partial R} + \frac{2nu}{R} = 0\,, \tag{19}$$

$$\frac{\partial nu}{\partial t} + \frac{\partial}{\partial R}\left[n(u^2+c^2)\right] + \frac{2nu^2}{R} = 0\,, \tag{20}$$

$$\frac{\partial n_{\rm HI}}{\partial t} + \frac{\partial n_{\rm HI}u}{\partial R} + \frac{2n_{\rm HI}u}{R} = (n-n_{\rm HI})^2\alpha_{\rm H} - n_{\rm HI}\phi\,, \tag{21}$$

$$\phi = \frac{S_*\sigma_{\nu_0}}{4\pi R^2}e^{-\tau_{\nu_0}}\,; \qquad \tau_{\nu_0} = \sigma_{\nu_0}\int_0^R n_{\rm HI}\,dR'\,, \tag{22}$$

where R is the spherical radius, u the (radial) fluid velocity, n is the number density of the (pure H) gas, $n_{\rm HI}$ is the neutral H number density, $n - n_{\rm HI}$ is the ionized H density (equal to the electron density), and $\alpha_{\rm H} = 2.59\times10^{-13}$ cm^3 s^{-1} is the case B recombination coefficient of H at 10^4 K. The photoionization rate ϕ is computed in the standard "grey HII region" approximation (in which the frequency dependence of the photoionization cross section σ_ν is not considered), so that it is given (as a function of the ionizing photon rate S_* and the Lyman limit HI photoionization cross section $\sigma_{\nu_0} = 6.3\times10^{-18}$ cm^2) by equation (22). Finally, the sound speed is computed as a function of the neutral fraction of the gas as:

$$c = \left(\frac{n_{\rm HI}}{n_{\rm H}}\right)c_0 + \left(1-\frac{n_{\rm HI}}{n_{\rm H}}\right)c_i\,, \tag{23}$$

where c_i is the isothermal sound speed of the ionized gas and c_0 is the sound speed of the external, neutral gas.

The code used to integrate these equations is described by Raga et al. (2012), and has a second order (space and time) implementation of the "flux vector splitting" algorithm of van Leer (1982). With this code, we have run four models with the parameters given in Table 1, using a 2000 point, uniform radial grid of outer radius $R_{\rm out}$, fully containing all of

TABLE 1

PARAMETERS OF THE HII REGION SIMULATIONS

Models	M1	M2	M3	M4
n_0 [cm^{-3}]	10^7	10^7	100	10
c_0 [km s^{-1}]	1.0	0.316	1.0	1.0
$R_{\rm out}$ [cm]	1.0×10^{18}	3.0×10^{18}	2.0×10^{21}	8.0×10^{21}
R_S [cm]	4.52×10^{15}	4.52×10^{15}	9.73×10^{18}	4.52×10^{19}
R_f [cm]	9.73×10^{16}	4.52×10^{17}	2.10×10^{20}	9.73×10^{20}
σ	0.01	0.001	0.01	0.01
λ	11699	11699	252	117
$(R_S n_0 \sigma_{\nu_0})^{-1}$	3.5×10^{-6}	3.5×10^{-6}	1.6×10^{-4}	3.5×10^{-4}

the perturbations within the computational domain during the time-integration.

The four models share a $S_* = 10^{49}$ s^{-1} stellar photoionization rate (corresponding to an O7, main sequence star) and a $c_i = 10$ km s^{-1} ionized gas sound speed (see equation 23). The different values chosen for the environmental density n_0 (see Table 1) range from 10^7 cm^{-3} (appropriate for an ultracompact HII region) down to 10 cm^{-3}. Model M1 has been previously presented by Raga et al. (2012).

These densities result in values for the dimensionless parameter λ (see equations 10 and 11) in the $\sim$100–10^4 range (see Table 1). Also, two values of the environmental sound speed c_0 (1.0 and 0.316 km s^{-1}) have been explored, resulting in values of the dimensionless parameter σ (see equation 10) of 0.01 and 0.001, respectively (see Table 1).

3.2. *Comparison of model M1 with the thin shell solutions*

In Figure 2, we present the density stratification in the (t, R)-plane resulting from model M1 (which is appropriate for an ultracompact HII region, see Table 1). This stratification shows the low density, expanding HII region (lower part of the figure) and the shock driven by the expansion into the neutral enviromnent. In this figure we have plotted Dyson's solution and the solution of Raga et al. (2012), both of which neglect the inertia of the shocked, neutral layer. The solution of Raga et al. (2012) coincides with Dyson's solution at low values of t, but it converges to the correct, final radius R_f for large times. This solution does not have the "overshoot" shown by the numerical simulation (i.e., at times $t \sim 5 \times 10^4$ yr, the HII region has radii larger than R_f, see Figure 2).

Also shown in Figure 2 are a numerical integration of the thin-shell model (equations 8–9) and the analytic solution given by equation (15). We see that the numerical, thin shell solution has a larger overshoot region (with $R > R_f$), and that it has a pronounced rebound which is completely absent in the numerical simulation. This lack of agreement between the numerical simulation and the thin shell solution is not surprising, given the fact that at

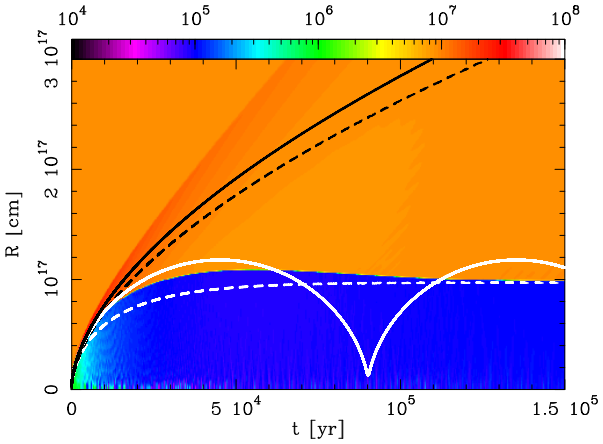

Fig. 2. (t, R)-plane density stratification obtained from model M1. The ion+atom number density is shown (in cm^{-3}) with the colour scheme given by the top bar. As time evolves, the radius of the low density, HII region (blue region in the bottom part of the plot) first grows and then settles to the final radius (R_f) resulting from the HII region/surrounding environment pressure equilibrium condition (see equation 2). The plot shows Dyson's solution (black dashed line) and the solution of Raga et al. (2012) (white dashed line), both of which do not include the inertia of the neutral, swept-up material (see § 1). The analytic, thin shell solution given by equation (15) (black solid line) and the results of a numerical integration of equations (8–9) (white solid line) are also shown. The color figure can be viewed online.

$t \sim 5 \times 10^4$ yr the width of the perturbed, neutral region (this is the region between the outer edge of the HII region and the outer shock, see Figure 2) is already comparable to the HII region radius. Therefore, a thin shell model is clearly not applicable at the later evolutionary times shown in Figure 2.

In Figure 3, we show a zoom (in the t, R-plane) of the early evolution of model M1. In this plot, we see that for $t < 3000$ yr the analytic and numerical thin shell solutions are indistinguishable, and that they agree very well with the expanding HII region predicted from the numerical simulation. At these times, Dyson's solution and the solution of Raga et al. (2012) predict lower radii than the ones of the simulated HII region (see Figure 3). At larger times, the HII region radius predicted from the numerical simulation deviates from all of the other solutions.

From the comparison of model M1 with the other more approximate models we therefore conclude:

- the numerical, thin shell solutions (see Figures 1 and 2) show a first overshoot of the final HII region radius R_f which is too large. The successive "rebounds" of the thin shell solutions are not physical, and they occur at times in which the numerical simulation shows that the shocked, neutral environment is not confined to a thin shell (so that the thin shell model is meaningless),

- at early evolutionary times (see Figure 3), both the numerical and analytic, thin shell solutions show an excellent agreement with model M1. The fact that they are clearly better than Dyson's solution shows that a more accurate model for the early time-evolution is obtained when the inertia of the shocked, neutral environment is included in the model.

3.3. *The universal, expanding HII region solution*

We have computed four HII region simulations (models M1–M4, see Table 1) in order to explore the following possibility. In § 2.3, we have shown that for a combination of dimensionless parameters (see equations 10 and 11) that satisfies the conditions $\lambda \gg 1$ and $\sigma \ll 1$, there is a single solution of R/R_f as a function of $\tau = tc_0/R_f$ which is valid for all models (satisfying the above conditions).

Clearly, in the set of equations used for the numerical simulations (equations 19–22), it is possible to define other dimensionless numbers. In particular, let us consider the dimensionless number $(R_S n_0 \sigma_{\nu_0})^{-1}$ (see equation 22). This number measures the thickness of the ionization front transition

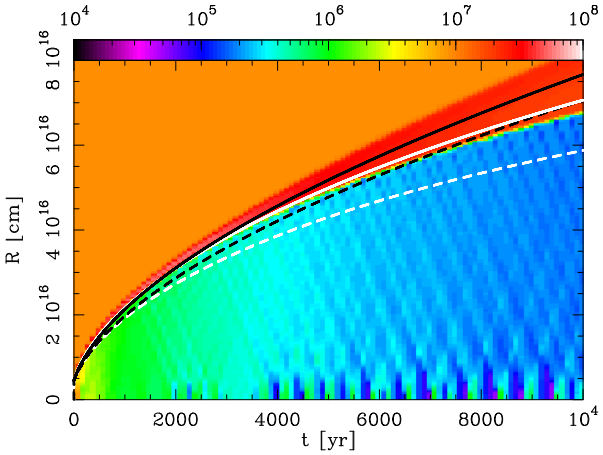

Fig. 3. (t, R)-plane density stratification obtained from model M1. This is a zoom of the initial expansion region of the density stratification shown in Figure 2. The color figure can be viewed online.

in units of the initial Strömgren radius (equation 1) of the HII region, and has a value $\ll 1$ for all models (see Table 1) as well as for all real HII regions produced by stellar sources. Therefore, the ionization front is extremely narrow, and the precise value of its thickness is unlikely to affect the dynamics of the HII region expansion.

Therefore, it might be reasonable to assume that the expansion of the simulated HII regions is mostly determined by the σ and λ dimensionless parameters (see equation 10), and that it also has a "high λ, low σ" regime with a universal R/R_f vs. $\tau = tc_0/R_f$ law (where R is the radius of the expanding HII region). To explore this possibility, in Figure 4 we show the density stratifications in the dimensionless $(R/R_f, \tau)$-plane obtained from models M1–M4.

It is clear from Figure 4 that all of the computed models produce a very similar HII region expansion, regardless of the model parameters. This is shown more quantitatively in Figure 5, in which we plot the HII region radius (calculated as the position at which H is 50% ionized) as a function of (dimensionless) time for all models.

The two models with $\lambda \sim 10^4$ (M1 and M2, with σ values of 0.01 and 0.001, respectively, see Table 1) show indistinguishable expansion laws. The models with lower values of λ (M3 and M4, with $\lambda \sim 250$ and 100, respectively) show solutions with small but progressively larger deviations from model M1 (see Figure 3).

Therefore, it is clear that the numerical simulations do show a "high λ, low σ" regime, in which all models share very similar R/R_f vs. $\tau = tc_0/R_f$ HII

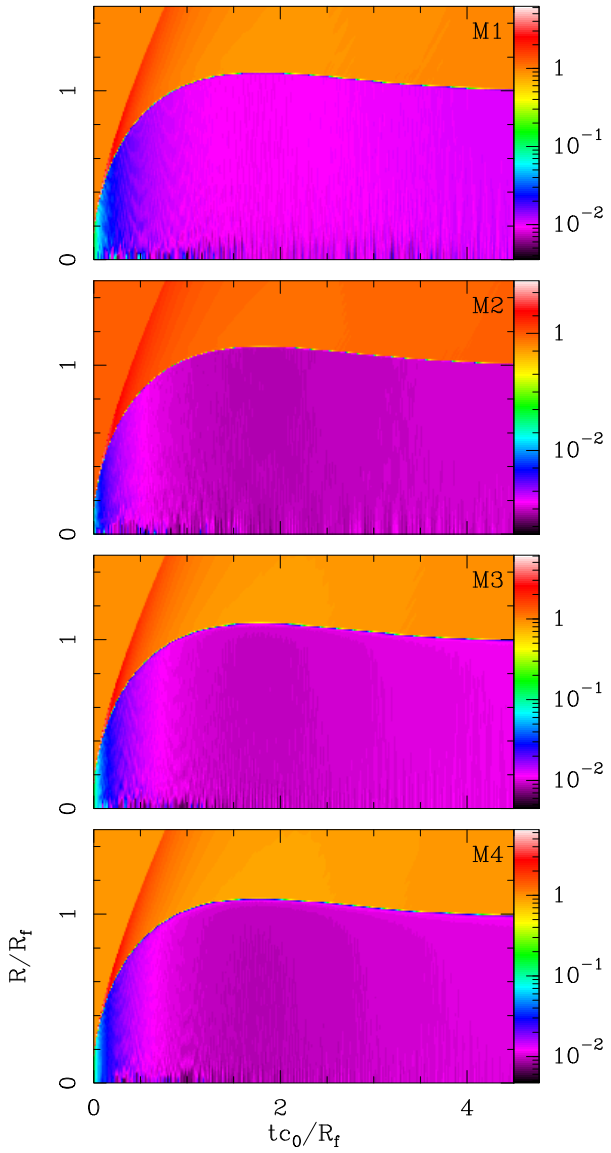

Fig. 4. Density stratifications in the (t, R)-plane obtained from models M1 (top) to M4 (bottom). The time axis is given in units of R_f/c_0 (the ratio between the final radius of the HII region and the isothermal sound speed of the neutral environment) and the radial axis in units of R_f. The densities are given (in units of the environmental density n_0) by the bars on the right of each plot. Model M2 (which has a smaller value of $\sigma = (c_0/c_i)^2$) shows a larger density range than the other models. The color figure can be viewed online.

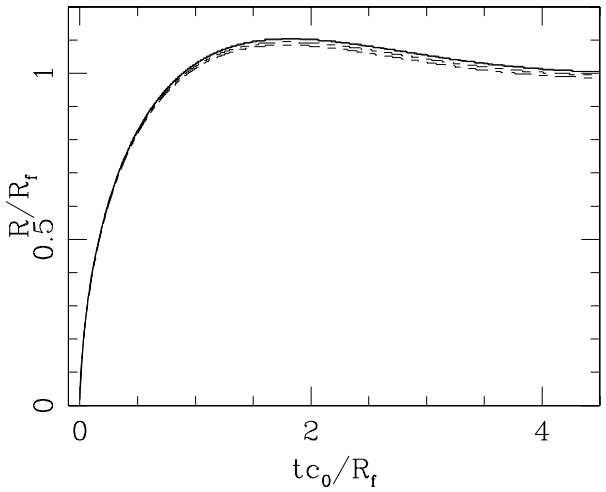

Fig. 5. Radius of the HII region (in units of R_f) vs. time (in units of R_f/c_0) obtained from the four numerical simulations (see Table 1). The results from models M1 and M2 are shown with solid curves, and the results from M3 and M4 with dashed curves. The lower curve corresponds to model M4.

TABLE 2

EXPANSION LAW FOR $\lambda \gg 1$, $\sigma \ll 1$

tc_0/R_f	R/R_f	v/c_0
0.1	0.38	2.01
0.2	0.55	1.34
0.3	0.67	1.00
0.4	0.76	0.88
0.5	0.83	0.75
0.7	0.93	0.44
1.0	1.03	0.23
1.5	1.10	0.07
2.0	1.10	−0.02
2.5	1.08	−0.06
3.0	1.06	−0.05
3.5	1.03	−0.04
4.0	1.02	−0.03
4.5	1.01	−0.01
5.0	1.00	0.00

region expansion laws. This "universal law" is tabulated in Table 2, in which we give the values of R/R_f as a function of $\tau = tc_0/R_f$ obtained from model M2 (our model with highest λ and lowest σ values). Actually, the HII region expansions produced by models M1 and M2 agree to within the number of digits shown in Table 2.

We do not tabulate the solution for low values of the dimensionless time $\tau = tc_0/R_f$. For such low values of τ the analytic, thin shell solution (equation 15) should be used, as it gives results which agree very well with the numerical simulations.

In this way, the HII region radius as a function of time can be obtained by scaling the solution given in Table 1 using the appropriate values for the environmental (isothermal) sound speed c_0 and for the final HII region radius R_f (see equation 2). The resulting HII region radius as a function of time will be a good approximation to the real expansion of the nebula if the conditions $\lambda \gg 1$ and $\sigma \ll 1$ (see equation 10) are met.

In Table 2 we also give the dimensionless expansion velocity v/c_0 corresponding to the "universal solution". We see that during most of its evolution to pressure equilibrium, the HII region expands quite slowly, at velocities comparable to, or smaller than, the isothermal sound speed of the neutral gas. This may explain why this expansion has been difficult to detect observationally.

Finally, we propose an interpolation formula that reproduces the "universal solution" (see Table 1) with an accuracy of better than 2% in R/R_f:

$$f_1(\tau) = \left(\frac{7}{2\sqrt{3}}\tau\right)^{4/7}, \tag{24}$$

$$f_2(\tau) = 1 - \left(1 - 2.2\tau + 4.2\tau^2 - 3.3\tau^3\right) e^{-2.4\tau}, \tag{25}$$

$$\frac{R}{R_f}(\tau) = e^{-10\tau} f_1(\tau) + (1 - e^{-10\tau}) f_2(\tau), \tag{26}$$

where $f_1(\tau)$ is the $\sigma \ll 1$ limit of the analytic, thin shell solution (see equation 15) and $f_2(\tau)$ is a least squares fit to the numerical solution given in Table 2. An appropriate switch between the analytic, small τ solution and the least squares fit is achieved with the $e^{-10\tau}$ weight (see equation 26).

4. SUMMARY

We present a new, thin shell model for the expansion of an HII region. The solutions depend on two dimensionless numbers: λ and σ (see equation 10). The σ parameter ($\sim$0.01 for typical sound speeds $c_0 \approx 1$ km s^{-1} and $c_i \approx 10$ km s^{-1}) is the square of the neutral-to-ionized gas sound speed ratio, and the λ parameter is the ratio between the sound crossing time and the recombination timescale of the initial Strömgren sphere. For HII regions powered by O stars in environments of number densities $n_0 \geq 1$ cm^{-3}, one always has $\lambda > 10$ (see equation 11).

We show that for $\lambda \gg 1$ (a condition met in observed HII regions, see above), the thin shell model simplifies from two to one differential equation (equation 14), which can be integrated analytically for the $\sigma = 0$ case. We also show that if the conditions $\lambda \gg 1$ and $\sigma \ll 1$ are met, and an appropriate adimensionalization is used, a single, "universal solution" for the thin shell HII region expansion model is obtained (equations 16 and 18).

We have carried out spherically symmetric, gasdynamic simulations of the expansion of HII regions which show a good agreement with the thin shell models for the beginning of the expansion. At later times, the shocked, neutral medium pushed out by the HII region becomes "thick" (i.e., with a width comparable and then larger than the outer radius of the HII region), and the numerical simulations deviate very substantially from the predictions of the thin shell model (which show a series of compressions and re-expansions which are absent in the numerical simulations).

We have computed a series of numerical simulations with dimensionless parameters σ=0.001–0.01 and $\lambda \sim$100–10^4 (see Table 1). We find that if the dimensionless HII region radius R/R_f (obtained from the numerical simulations) is plotted as a function of dimensionless time tc_0/R_f (where c_0 is the environmental sound speed and R_f the final, pressure equilibrium radius of the HII region), most similar expansion laws are found for all of the computed models (see Figure 5). This result shows that a high λ, low σ "universal expansion law" is also found in the simulated expanding HII regions. This solution has been tabulated, and it can be scaled so as to model the time-evolution of any given HII region (see Table 2).

In this way, we show that spherically symmetric, gasdynamic models of HII regions share the existence of a "high λ, low σ" regime with the thin shell formulation. The existence of this regime considerably simplifies the interpretation of observations of expanding HII regions.

We acknowledge support from the Conacyt grants 61547, 101356 and 101975. We thank an anonymous referee for pointing out a series of mistakes in the first version of this paper.

REFERENCES

de Pree, C. G., Rodríguez, L. F., & Goss, W. M. 1995, RevMexAA, 31, 39

Dyson, J. E., & Williams, D. A. 1980, The Physics of the Interstellar Medium (Manchester: Manchester Univ. Press)

Franco, J., Tenorio-Tagle, G., & Bodenheimer, P. 1990, ApJ, 349, 126

Kurtz, S. 2005, in IAU Symp. 227, Massive Star Birth: A Crossroads of Astrophysics, ed. R. Cesaroni, M. Felli, E. Churchwell, & M. Walmsley (Cambridge: Cambridge Univ. Press), 111

Mathews, W. G., & O'Dell, C. R. 1969, ARA&A, 7, 67
Raga, A. C., Cantó, J., & Rodríguez, L. F. 2012, MNRAS, 419, L39
Shu, F. H., Lizano, S., Galli, D., Cantó, J., & Laughlin, G. 2002, ApJ, 580, 969
Spitzer, L. 1968, Diffuse Matter in Space (New York: Interscience)
Tenorio-Tagle, G., Beltrametti, M., Bodenheimer, P., & Yorke, H. W. 1982, A&A, 112, 104
van Leer, B. 1982, ICASE Report No. 82-30

A. C. Raga: Instituto de Ciencias Nucleares, Universidad Nacional Autónoma de México, Apdo. Postal 70-543, 04510 D.F., Mexico (raga@nucleares.unam.mx).
J. Cantó, Instituto de Astronomía, Universidad Nacional Autónoma de México, Apdo. Postal 70-242, 04510 D.F., Mexico.
L. F. Rodríguez: Centro de Radiostronomía y Astrofísica, Universidad Nacional Autónoma de México, Apdo. Postal 3-72, (Xangari), 58089 Morelia, Michoacán, Mexico (l.rodriguez@astrosmo.unam.mx).